Equations of Motion for Maneuvering Flexible Spacecraft

L. Meirovitch* and R.D. Quinn†
Virginia Polytechnic Institute and State University, Blacksburg, Virginia

This paper is concerned with the derivation of the equations of motion for maneuvering flexible spacecraft both in orbit and in an Earth-based laboratory. The structure is assumed to undergo large rigid-body maneuvers and small elastic deformations. A perturbation approach is presented in which the quantities defining the rigid-body maneuver are regarded as the unperturbed motion and the elastic motions and deviations from the rigid-body motions are regarded as the perturbed motion. The perturbation equations are linear, non-self-adjoint, and with time-dependent coefficients. A maneuver force distribution exciting the least amount of elastic deformation of the spacecraft is developed. Numerical results highlight the vibration caused by rotational maneuvers.

I. Introduction

THE problem of simultaneous maneuver and vibration suppression of a flexible spacecraft is becoming increasingly important. Some studies carried out by NASA involve experiments consisting of the control of flexible bodies carried by a shuttle in an Earth orbit. Other missions involve Earth-based laboratory simulations of similar experiments. Hence, a formulation capable of accommodating both types of experiments is desirable. To this end, we propose to derive the equations of motion for the spacecraft of Fig. 1 regarding the structure as orbiting the Earth and then modify these equations to describe the laboratory experiment of Fig. 2.

NASA is currently involved in two experimental programs to test techniques proposed for active control of space structures. The first is ground-based and is known as the Spacecraft Control Laboratory Experiment (SCOLE). Ground-based experimentation has its limitations because it is almost impossible to duplicate the space environment in a laboratory. The second is known as Control of Flexible Spacecraft (COFS) and involves experiments with control of flexible bodies carried by a shuttle in an Earth orbit. The same project also includes laboratory simulations of similar experiments, which will precede the space experiments. Testing a control technique in space is expensive, and deploying an unproven system could be disastrous. Hence, mathematical modeling and computer simulation are valuable in assuring the success of both SCOLE and COFS.

Early spacecraft were mostly rigid, and their attitude motion was controlled by passive means, such as spin stabilization or gravity-gradient stabilization. Reference 1 represents one of the first works in which the equations of motion of spinning spacecraft consisting of a rigid body with flexible appendages were derived. About the same time, in the mid-1960s, a formalism was being developed for deriving the attitude equations of motion of a spacecraft consisting of a number of interconnected rigid bodies arranged in a "topological tree."[2,3] The formalism was extended to the case in which the interconnected bodies were flexible[4-7] and to the case in which the spacecraft is stabilized by means of active control.[8,9]

Another approach to the derivation of the equations of motion, suitable not only for spacecraft structures but also for aircraft and civil structures, is known as component-mode synthesis or substructure synthesis.[10-15] This approach regards the structures as a collection of substructures, each one represented by a limited number of degrees of freedom. Hence, the method represents not only a modeling technique but a truncation procedure as well. It should be observed that the approach of Ref. 1 can be regarded as an example of substructure synthesis although it was not identified as such. Examples of control of structures modeled by substructure synthesis can be found in Refs. 16-20.

A problem of particular interest is the slewing of a spacecraft. The equations of motion governing the slewing of a rigid body are well known.[21] References 22-24 address the problem of single-axis rotational maneuver and simultaneous vibration suppression of a spacecraft consisting of a rigid core with a number of flexible booms vibrating in a plane normal to the spin axis. These references have in common that they all represent extensions of rigid-body maneuvering techniques, requiring the solution of a two-point boundary-value problem. The maneuver and vibration control problems are coupled, and numerical difficulties arise as the order of the system increases.[23]

This paper is concerned with the more general case of all slewing and vibration suppression of a flexible spacecraft of the type shown in Fig. 1. The equations of motion are derived using a Lagrangian approach in conjunction with substructure synthesis. In the derivation of the equations of motion for the system of Fig. 1, the shuttle is treated as a rigid body, and the beam and antenna, as well as the supporting cable in the case of the laboratory experiment, are treated as distributed-parameter members. The results can easily be extended to structures with multiple flexible appendages.[25]

The equations describing the motion of a rigid spacecraft are nonlinear ordinary differential equations. On the other hand, the equations describing the small elastic displacements of a flexible spacecraft relative to a frame embedded in the undeformed spacecraft are linear partial differential equations. Hence, the complete equations describing a flexible spacecraft during a certain maneuver represent a set of nonlinear hybrid differential equations. In general, hybrid systems of equations do not permit closed-form solution, so that one must consider an approximate solution. This implies spatial discretization and truncation, which can be carried out by representing the elastic motion in terms of a finite set of admissible functions.

The discretized equations of motion of a spacecraft during a maneuver represent a set of simultaneous nonlinear ordinary differential equations, where the nonlinearity is due to the

Received Jan. 13, 1986; revision received Oct. 6, 1986.

*University Distinguished Professor. Fellow AIAA.

†Graduate Research Assistant, Department of Engineering Science and Mechanics; currently, Assistant Professor, Department of Mechanical and Aerospace Engineering, Case Western Reserve University, Cleveland, OH.

large rigid-body motions. A perturbation approach can be used to reduce the equations of motion to a form that lends itself to a more efficient treatment. This technique amounts to separating the equations of motion into a set of equations governing the rigid-body motions, representing the unperturbed system, and a set of time-varying linear equations governing small elastic motions and deviations from the prescribed rigid-body maneuver, representing the perturbation. The perturbation technique permits a rigid-body maneuver strategy that is independent of the elastic analysis. The perturbation equations are linear equations with time-varying coefficients, where the coefficients are known as soon as the rigid-body maneuver policy associated with the unperturbed system has been determined.

The force distribution producing the desired maneuver and causing the least amount of vibration is derived. The perturbation vibration equations are simplified using a truncated set of premaneuver eigenvectors as admissible vectors. The resulting equations are referred to as the *quasi-modal equations* of motion.

II. Equations of Motion of the Spacecraft

It is convenient to refer the motion of the spacecraft to a given reference frame $x_0y_0z_0$, where the frame can be regarded as being embedded in the rigid shuttle. The motion of the reference frame is characterized by six degrees of freedom, three rigid-body translations, and three rigid-body rotations. The elastic motion is measured relative to the rigid frame and is characterized by an infinite number of degrees of freedom.

We propose to derive the equations of motion by means of the Lagrangian approach. To this end, we must first obtain expressions for the kinetic energy, the potential energy, and the virtual work. Considering Fig. 1 and denoting the position of the origin 0 of the frame $x_0y_0z_0$ by the vector $\boldsymbol{R}$ and the position of a point S on the shuttle relative to 0 by $\boldsymbol{r}$, the position of S relative to the inertial frame XYZ is $\boldsymbol{R}_S=\boldsymbol{R}+\boldsymbol{r}$. Moreover, denoting the vector from 0 to a nominal point A on a typical elastic appendage by $\boldsymbol{a}$ and the elastic displacement vector of point A by $\boldsymbol{u}$, the inertial position of A in the displaced configuration is $\boldsymbol{R}_A=\boldsymbol{R}+\boldsymbol{a}+\boldsymbol{u}$. It must be noted that the vectors $\boldsymbol{R}$, $\boldsymbol{a}$, and $\boldsymbol{u}$ are likely to be measured relative to axes $x_0y_0z_0$. In view of the above, the velocity of a point S on the shuttle and that of a point A on the appendage are

$$\dot{\boldsymbol{R}}_S=\dot{\boldsymbol{R}}+\boldsymbol{\omega}\times\boldsymbol{r} \tag{1a}$$

$$\dot{\boldsymbol{R}}_A=\dot{\boldsymbol{R}}+\boldsymbol{\omega}\times(\boldsymbol{a}+\boldsymbol{u})+\dot{\boldsymbol{u}} \tag{1b}$$

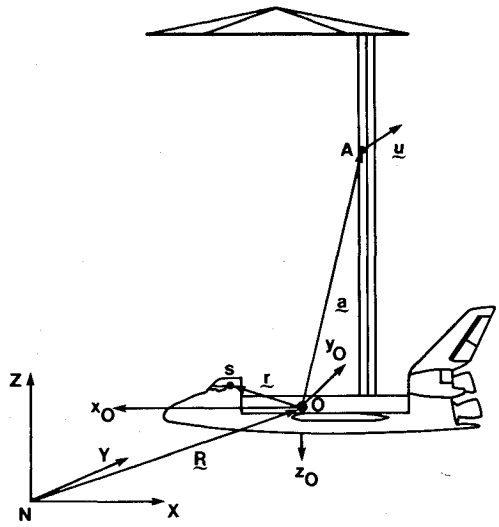

Fig. 1 Earth-orbiting spacecraft.

$\dot{\boldsymbol{R}}$ is the translational velocity, $\boldsymbol{\omega}$ the angular velocity of the frame $x_0y_0z_0$ with respect to the inertial space, and $\dot{\boldsymbol{u}}$ the elastic velocity of the point A relative to the $x_0y_0z_0$ frame. Hence, the kinetic energy of the spacecraft is

$$\begin{aligned}
T&=\frac{1}{2}\int_{m_S}|\dot{\boldsymbol{R}}_S|^2dm_S+\frac{1}{2}\int_{m_A}|\dot{\boldsymbol{R}}_A|^2dm_A\\
&=\frac{1}{2}\int_{m_S}|\dot{\boldsymbol{R}}+\boldsymbol{\omega}\times\boldsymbol{r}|^2dm_S\\
&+\frac{1}{2}\int_{m_A}|\dot{\boldsymbol{R}}+\boldsymbol{\omega}\times(\boldsymbol{a}+\boldsymbol{u})+\dot{\boldsymbol{u}}|^2dm_A\\
&=\frac{1}{2}m|\dot{\boldsymbol{R}}|^2+\frac{1}{2}\boldsymbol{\omega}^TI_0\boldsymbol{\omega}+\dot{\boldsymbol{R}}\cdot(\boldsymbol{\omega}\times\boldsymbol{S}_0)\\
&+\frac{1}{2}\int_{m_A}|\dot{\boldsymbol{u}}|^2dm_A+\dot{\boldsymbol{R}}\cdot\left(\int_{m_A}\dot{\boldsymbol{u}}dm_A\right.\\
&\left.+\boldsymbol{\omega}\times\int_{m_A}\boldsymbol{u}dm_A\right)+\int_{m_A}\dot{\boldsymbol{u}}\cdot(\boldsymbol{\omega}\times\boldsymbol{a})dm_A\\
&+\int_{m_A}(\boldsymbol{\omega}\times\boldsymbol{a})\cdot(\boldsymbol{\omega}\times\boldsymbol{u})dm_A\\
&+\frac{1}{2}\int_{m_A}|\boldsymbol{\omega}\times\boldsymbol{u}|^2dm_A+\int_{m_A}\dot{\boldsymbol{u}}\cdot(\boldsymbol{\omega}\times\boldsymbol{u})dm
\end{aligned} \tag{2}$$

where

$$\boldsymbol{S}_0=\int_{m_S}\boldsymbol{r}dm_S+\int_{m_A}\boldsymbol{a}dm_A \tag{3}$$

and m_S, m_A, and m are the masses of the shuttle, the appendage, and the entire spacecraft, respectively. Also, I_0 is the total mass moment of inertia matrix of the undeformed structure about point 0. Note that $|\boldsymbol{x}|^2$ denotes the inner product $\boldsymbol{x}\cdot\boldsymbol{x}$.

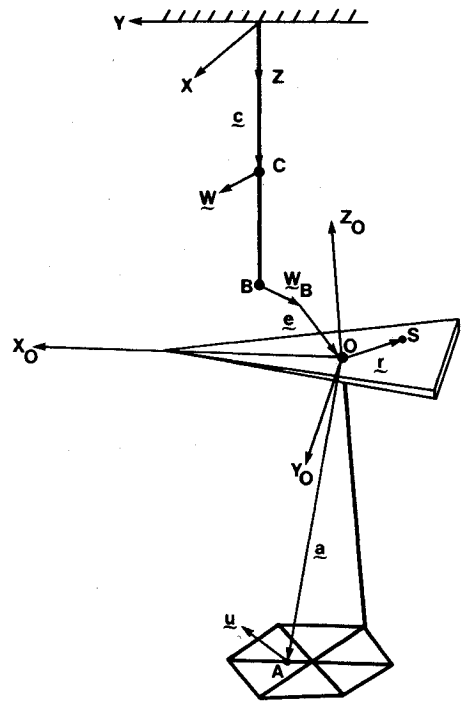

Fig. 2 SCOLE configuration.

The potential energy is due to the combined effects of gravity and strain energy. Assuming that the origin of the inertial coordinate system coincides with the center of the gravitational field, namely, the center of the Earth, the gravitational potential energy can be expressed as

$$V_g = -Gm_e\left(\int_{m_S} |\boldsymbol{R}+\boldsymbol{r}|^{-1}\mathrm{d}m_S + \int_{m_A} |\boldsymbol{R}+\boldsymbol{a}+\boldsymbol{u}|^{-1}\mathrm{d}m_A\right) \tag{4}$$

where m_e is the mass of the Earth and G the universal gravitational constant. The strain energy can be expressed as an energy inner product denoted by $[,]$.[26] The total potential energy then becomes

$$V = \frac{1}{2}[\boldsymbol{u},\boldsymbol{u}] + V_g \tag{5}$$

Note that $[\boldsymbol{u},\boldsymbol{u}]$ contains the potential energy due to centrifugal and gravitational stiffening effects.[26]

The virtual work is due to external forces, including control forces. Denoting by $\boldsymbol{f}_S$ the force vector per unit volume of the shuttle and by $\boldsymbol{f}_A$ the force vector per unit volume of the appendage, we can write the virtual work as

$$\delta W = \int_{D_S} \boldsymbol{f}_S \cdot \delta\boldsymbol{R}_S \mathrm{d}D_S + \int_{D_A} \boldsymbol{f}_A \cdot \delta\boldsymbol{R}_A \mathrm{d}D_A \tag{6}$$

where D_S and D_A are the domains of the shuttle and appendage, respectively.

Next, we propose to discretize the system in space. To this end, we express the elastic displacement vector in the form

$$\boldsymbol{u} = \Phi\boldsymbol{q} \tag{7}$$

where Φ is a matrix of space-dependent admissible functions[26] and $\boldsymbol{q}$ a vector of time-dependent generalized coordinates. Introducing Eq. (7) into Eq. (2), the kinetic energy can be expressed in the matrix form

$$\begin{aligned} T = {} & \frac{1}{2}m\dot{\boldsymbol{R}}^T\dot{\boldsymbol{R}} + \frac{1}{2}\boldsymbol{\omega}^T I_0\boldsymbol{\omega} + \dot{\boldsymbol{R}}^T C^T\tilde{S}_0\boldsymbol{\omega} \\ & + \frac{1}{2}\dot{\boldsymbol{q}}^T M_A\dot{\boldsymbol{q}} + \dot{\boldsymbol{R}}^T C^T\bar{\Phi}\dot{\boldsymbol{q}} + \dot{\boldsymbol{R}}^T C^T\tilde{\boldsymbol{\omega}}^T\bar{\Phi}\boldsymbol{q} \\ & + \dot{\boldsymbol{q}}^T\bar{\Phi}^T\boldsymbol{\omega} + \boldsymbol{\omega}^T\int_{m_A}\tilde{\boldsymbol{a}}^T\tilde{\boldsymbol{\omega}}^T\Phi\mathrm{d}m_A\boldsymbol{q} \\ & - \frac{1}{2}\boldsymbol{q}^T\tilde{L}_A(\boldsymbol{\omega})\boldsymbol{q} + \dot{\boldsymbol{q}}^T\bar{L}_A(\boldsymbol{\omega})\boldsymbol{q} \end{aligned} \tag{8}$$

where

$$\bar{\Phi} = \int_{m_A}\Phi\mathrm{d}m_A \tag{9a}$$

$$\tilde{\Phi}^T = \int_{m_A}\Phi^T\tilde{\boldsymbol{a}}\mathrm{d}m_A \tag{9b}$$

$$\tilde{L}_A(\boldsymbol{\omega}) = \int_{m_A}\Phi^T\tilde{\boldsymbol{\omega}}^T\Phi\mathrm{d}m_A \tag{9c}$$

$$\bar{L}_A(\boldsymbol{\omega}) = \int_{m_A}\Phi^T\tilde{\boldsymbol{\omega}}^2\Phi\mathrm{d}m_A \tag{9d}$$

$$M_A = \int_{m_A}\Phi^T\Phi\mathrm{d}m_A \tag{9e}$$

The matrix M_A can be identified as the mass matrix of the appendage. The symbol C represents a rotation matrix from the inertial frame XYZ to the $x_0y_0z_0$ frame, and its elements are nonlinear functions of Euler's angles α. The tilde over a typical vector $\boldsymbol{v}$ denotes a skew symmetric matrix of the form

$$\tilde{\boldsymbol{v}} = \begin{bmatrix} 0 & v_z & -v_y \\ -v_z & 0 & v_x \\ v_y & -v_x & 0 \end{bmatrix} \tag{10}$$

Recognizing that the magnitude of $\boldsymbol{R}$ is large and that of $\boldsymbol{u}$ small in comparison with the magnitude of the other vectors in Eq. (4) and ignoring terms of higher order, a binomial expansion permits us to write

$$\begin{aligned} V_g \cong {} & -Gm_e\left\{m|\boldsymbol{R}|^{-1} - \boldsymbol{R}\cdot\left(S_0 + \int_{m_A}\boldsymbol{u}\mathrm{d}m_A\right)|\boldsymbol{R}|^{-3}\right. \\ & + \frac{1}{2}|\boldsymbol{R}|^{-5}\left[\int_{m_S}(3\boldsymbol{r}^T CRR^T C^T\boldsymbol{r} - \boldsymbol{r}^T\boldsymbol{r})\mathrm{d}m_S\right. \\ & \left.\left. + \int_{m_A}(3\boldsymbol{a}^T CRR^T C^T\boldsymbol{a} - \boldsymbol{a}^T\boldsymbol{a})\mathrm{d}m_A\right]\right\} \end{aligned} \tag{11}$$

Introducing Eq. (11) into Eq. (5) and considering Eq. (7), the potential energy can be written in the form

$$\begin{aligned} V \cong {} & \frac{1}{2}\boldsymbol{q}^T K_A\boldsymbol{q} - Gm_e\left\{\frac{m}{|\boldsymbol{R}|} - \frac{1}{|\boldsymbol{R}|^2}\hat{\boldsymbol{R}}^T C^T(S_0 + \bar{\Phi}\boldsymbol{q})\right. \\ & \left. + \frac{1}{2|\boldsymbol{R}|^3}\left[3\hat{\boldsymbol{R}}^T C^T\bar{J}C\hat{\boldsymbol{R}} - \left(\int_{m_S}\boldsymbol{r}^T\boldsymbol{r}\mathrm{d}m_S + \int_{m_A}\boldsymbol{a}^T\boldsymbol{a}\mathrm{d}m_A\right)\right]\right\} \end{aligned} \tag{12}$$

where

$$K_A = [\Phi,\Phi] \tag{13a}$$

$$\hat{\boldsymbol{R}} = \frac{\boldsymbol{R}}{|\boldsymbol{R}|} \tag{13b}$$

$$\bar{J} = \int_{m_S}\boldsymbol{r}\boldsymbol{r}^T\mathrm{d}m_S + \int_{m_A}\boldsymbol{a}\boldsymbol{a}^T\mathrm{d}m_A \tag{13c}$$

are the stiffness matrix of the appendage, a unit vector in the direction of $\boldsymbol{R}$, and a matrix of inertia integrals, respectively. The position vector $\boldsymbol{R}$ and the corresponding equations of motion are expressed in the inertial frame, but the control forces are most conveniently represented in the 0 frame. Hence, the transformation matrix C must be employed in expressing the virtual work as follows:

$$\delta W = \boldsymbol{F}^T C\delta\boldsymbol{R} + \boldsymbol{M}^T D\delta\boldsymbol{\alpha} + \boldsymbol{Q}^T\delta\boldsymbol{q} \tag{14}$$

where

$$\boldsymbol{F} = \int_{D_S}\boldsymbol{f}_S\mathrm{d}D_S + \int_{D_A}\boldsymbol{f}_A\mathrm{d}D_A \tag{15a}$$

$$\boldsymbol{M} = \int_{D_S}\tilde{\boldsymbol{r}}^T\boldsymbol{f}_S\mathrm{d}D_S + \int_{D_A}\tilde{\boldsymbol{a}}^T\boldsymbol{f}_A\mathrm{d}D_A + \int_{D_A}\tilde{\boldsymbol{f}}_A\Phi\mathrm{d}D_A\boldsymbol{q} \tag{15b}$$

$$\boldsymbol{Q} = \int_{D_A}\Phi^T\boldsymbol{f}_A\mathrm{d}D_A \tag{15c}$$

are generalized force vectors in terms of components about x_0, y_0, and z_0 and $D = D(\alpha)$ is a matrix of trigonometric func-

tions of the Euler angles defined by the expression

$$\omega = D\dot{\alpha} \tag{16}$$

Lagrange's equations of motion can be written in the symbolic form

$$\frac{d}{dt}\left(\frac{\partial T}{\partial \dot{R}}\right) + \frac{\partial V}{\partial R} = C^T F \tag{17a}$$

$$\frac{d}{dt}\left(\frac{\partial T}{\partial \dot{\alpha}}\right) - \frac{\partial T}{\partial \alpha} + \frac{\partial V}{\partial \alpha} = D^T M \tag{17b}$$

$$\frac{d}{dt}\left(\frac{\partial T}{\partial \dot{q}}\right) - \frac{\partial T}{\partial q} + \frac{\partial V}{\partial q} = Q \tag{17c}$$

so that, considering Eqs. (8), (12), and (14) and premultiplying Eq. (17b) by D^{-T}, the equations of motion for the spacecraft in orbit are

$$m\ddot{R} + C^T\tilde{S}_0\dot{\omega} + C^T\tilde{\Phi}\ddot{q} + C^T\tilde{\omega}^T\tilde{S}_0\omega + 2C^T\tilde{\omega}^T\tilde{\Phi}\dot{q} + C^T(\tilde{\omega}^2 + \dot{\tilde{\omega}}^T)\tilde{\Phi}q + \frac{Gm_e}{|R|^3}\{mR + C^T(S_0 + \tilde{\Phi}q) - 3[\hat{R}\hat{R}^T C^T(S_0 + \tilde{\Phi}q)]\} = C^T F \tag{18a}$$

$$I_0\dot{\omega} + \tilde{\omega}^T I_0\omega + \tilde{S}_0^T C\ddot{R} + \tilde{\Phi}\ddot{q} + [\widetilde{C\ddot{R}}]\tilde{\Phi} + J(\dot{\omega}) + \tilde{\omega}^T J(\omega) + \frac{Gm_e}{|R|^3}[\widetilde{C\hat{R}}]\tilde{\Phi}]q + [\tilde{\omega}^T\tilde{\Phi} + J(\omega)]\dot{q} + \frac{Gm_e}{|R|^3}[\widetilde{C\hat{R}}]\left(S_0 + 3\bar{J}C\frac{\hat{R}}{|R|}\right) = M \tag{18b}$$

$$M_A\ddot{q} + \tilde{\Phi}^T C\ddot{R} + \tilde{\Phi}^T\dot{\omega} + \int_{m_A}\Phi^T\tilde{\omega}^T\tilde{a}\omega dm_A + \frac{Gm_e}{|R|^3}\tilde{\Phi}^T CR + \tilde{L}_A(\omega)\dot{q} + [\tilde{L}_A(\omega) + \tilde{L}_A(\dot{\omega}) + K_A]q = Q \tag{18c}$$

where we used the relation

$$\dot{C} = \tilde{\omega}C \tag{19a}$$

as well as the notation

$$J(\omega) = \int_{m_A}(\tilde{a}\tilde{\omega} + [\widetilde{a\omega}])\Phi dm_A \tag{19b}$$

The gravitational torque[27] is given by the last term on the left side of Eq. (18b). Note that premultiplying Eq. (17b) by D^{-T} is equivalent to considering Lagrange's equations in terms of quasi-coordinates.[27] Moreover, the position vector $\boldsymbol{R}$, its time derivatives, and the Euler angles $\alpha_1, \alpha_2, \alpha_3$ have been assumed to be of arbitrary magnitude, with the result that many nonlinear terms appear in Eqs. (18).

III. Equations of Motion for the Laboratory Experiment

In the laboratory experiment, the spacecraft is not actually free in space but is suspended from the ceiling by means of a cable. The support is likely to affect the dynamic characteristics of the system. Hence, in the sequel, the support is added to the free model in the form of a flexible member.

Considering Fig. 2, the position vector for an arbitrary point C on the cable is $\boldsymbol{R}_C = \boldsymbol{c} + \boldsymbol{w}$, where $\boldsymbol{c}$ is a position vector and $\boldsymbol{w}$ is the elastic displacement of the cable, both of which are measured with respect to the inertial frame. The position vector for the point 0 is $\boldsymbol{R} = \boldsymbol{c}_B + \boldsymbol{w}_B + \boldsymbol{e}$, where the subscript B denotes evaluation at the point B and $\boldsymbol{e}$ is the vector from point B (universal joint) to the point 0 fixed on the shuttle, measured with respect to the $x_0y_0z_0$ frame. Moreover, the position vectors of points on the shuttle and on the appendage are the same as for the unrestrained spacecraft, except that the expression for $\boldsymbol{R}$ is different here. The velocity vectors of an arbitrary point C on the cable and of point 0 are then

$$\dot{\boldsymbol{R}}_C = \dot{\boldsymbol{w}} \tag{20a}$$

$$\dot{\boldsymbol{R}} = \dot{\boldsymbol{w}}_B + \boldsymbol{\omega}\times\boldsymbol{e} \tag{20b}$$

The kinematics for the shuttle and appendage is similar to that for the unrestrained spacecraft in space. Hence, the kinetic energy for the entire structure is

$$\begin{aligned} T = {} & \frac{1}{2}\int_{m_C}|\dot{\boldsymbol{R}}_C|^2 dm_C + \frac{1}{2}\int_{m_S}|\dot{\boldsymbol{R}}_S|^2 dm_S \\ & + \frac{1}{2}\int_{m_A}|\dot{\boldsymbol{R}}_A|^2 dm_A = \frac{1}{2}\int_{m_C}|\dot{\boldsymbol{w}}|^2 dm_C \\ & + \frac{1}{2}\int_{m_S}|\dot{\boldsymbol{w}}_B + \boldsymbol{\omega}\times(\boldsymbol{e}+\boldsymbol{r})|^2 dm_S \\ & + \frac{1}{2}\int_{m_A}|\dot{\boldsymbol{w}}_B + \boldsymbol{\omega}\times(\boldsymbol{e}+\boldsymbol{a}+\boldsymbol{u}) + \dot{\boldsymbol{u}}|^2 dm_A \\ = {} & \frac{1}{2}\int_{m_C}|\dot{\boldsymbol{w}}|^2 dm_C + \frac{1}{2}m|\dot{\boldsymbol{w}}_B|^2 + \frac{1}{2}\omega^T I_0\omega \\ & + \frac{1}{2}m(\boldsymbol{\omega}\times\boldsymbol{e})\cdot(\boldsymbol{\omega}\times\boldsymbol{e}) + \dot{\boldsymbol{w}}_B\cdot(\boldsymbol{\omega}\times\boldsymbol{S}_B) \\ & + (\boldsymbol{\omega}\times\boldsymbol{e})\cdot(\boldsymbol{\omega}\times\boldsymbol{S}_0) + \frac{1}{2}\int_{m_A}|\dot{\boldsymbol{u}}|^2 dm_A \\ & + \dot{\boldsymbol{w}}_B\cdot\int_{m_A}\dot{\boldsymbol{u}}dm_A + \int_{m_A}\dot{\boldsymbol{u}}\cdot(\boldsymbol{\omega}\times\boldsymbol{b})dm_A \\ & + \int_{m_A}(\boldsymbol{\omega}\times\boldsymbol{b})\cdot(\boldsymbol{\omega}\times\boldsymbol{u})dm_A + \frac{1}{2}\int_{m_A}|\boldsymbol{\omega}\times\boldsymbol{u}|^2 dm_A \\ & + \int_{m_A}\dot{\boldsymbol{u}}\cdot(\boldsymbol{\omega}\times\boldsymbol{u})dm_A \end{aligned} \tag{21}$$

where

$$\boldsymbol{S}_B = \boldsymbol{S}_0 + m\boldsymbol{e} \tag{22a}$$

$$\boldsymbol{b} = \boldsymbol{a} + \boldsymbol{e} \tag{22b}$$

The elastic displacement vectors $\boldsymbol{u}$ and $\boldsymbol{w}$ have been assumed to be small.

The expression for the virtual work is given by Eq. (6), but the potential energy must be modified. The acceleration due to gravity is assumed to be constant now and to have the form $\boldsymbol{g} = -g\boldsymbol{u}_Z$, so that the gravitational potential is

$$V_g = \int_{m_C}(\boldsymbol{c}+\boldsymbol{w})\cdot\boldsymbol{g}dm_C + \int_{m_S}(\boldsymbol{R}+\boldsymbol{r})\cdot\boldsymbol{g}dm_S + \int_{m_A}(\boldsymbol{R}+\boldsymbol{a}+\boldsymbol{u})\cdot\boldsymbol{g}dm_A \tag{23}$$

where u_z is a unit vector in the Z direction. The total potential energy for the system can be expressed as

$$V=\frac{1}{2}[u,u]+\frac{1}{2}[w,w]+V_g \tag{24}$$

where $[w,w]$ is the energy inner product for the cable.

As with the appendage in the preceding section, the elastic displacement of the cable can be approximated by a linear combination of admissible functions, or

$$w=\psi\eta \tag{25}$$

where ψ is a matrix of space-dependent admissible functions and η is a vector of time-dependent generalized coordinates. Introducing Eqs. (7) and (25) into Eq. (21), the kinetic energy takes the matrix form

$$\begin{aligned}T=&\frac{1}{2}\dot\eta^T M_C\dot\eta+\frac{1}{2}\omega^T(I_0+m\tilde e^T\tilde e+2\tilde e^T\tilde S_0)\omega\\&+\dot\eta^T\psi_B^T C^T\tilde S_B\omega+\frac{1}{2}\dot q^T M_A\dot q+\dot\eta^T\psi_B^T C^T\bar\Phi\dot q\\&+\dot\eta^T\psi_B^T C^T\tilde\omega^T\bar\Phi q+\dot q^T\bar\Phi^T\omega+\omega^T\left[\int_{m_A}\tilde b\tilde\omega\Phi\,\mathrm{d}m_A\right]q\\&+\dot q^T\tilde L_A(\omega)q-\frac{1}{2}q^T\tilde L_A(\omega)q\end{aligned} \tag{26}$$

where

$$\bar\Phi^T=\int_{m_A}\Phi^T\tilde b\,\mathrm{d}m_A \tag{27a}$$

$$M_C=\int_{m_C}\psi^T\psi\,\mathrm{d}m_C+m\psi_B^T\psi_B \tag{27b}$$

The matrix M_C is the combined mass matrix of the cable and of the structure lumped at the end of the cable, in which ψ_B denotes the matrix ψ evaluated at B. Introducing Eqs. (7) and (25) into Eqs. (23) and (24), the potential energy can be written in the matrix form

$$\begin{aligned}V=&\eta^T\bar\psi^T g+S_B^T Cg+m\eta^T\psi_B^T g+q^T\bar\Phi^T Cg\\&+\frac{1}{2}q^T K_A q+\frac{1}{2}\eta^T K_C\eta\end{aligned} \tag{28}$$

where

$$\bar\psi=\int_{m_C}\psi\,\mathrm{d}m_C \tag{29a}$$

$$K_C=[\psi,\psi] \tag{29b}$$

in which K_C is the stiffness matrix of the cable. The virtual work can be expressed as

$$\delta W=F^T C\psi_B\delta\eta+M^T D\delta\alpha+Q^T\delta q \tag{30}$$

where all the terms have been defined previously.

Lagrange's equations remain in the symbolic form of Eqs. (17), with the exception of Eq. (17a), which must be replaced by

$$\frac{\mathrm{d}}{\mathrm{d}t}\left(\frac{\partial T}{\partial\dot\eta}\right)+\frac{\partial V}{\partial\eta}=\psi_B^T C^T F \tag{31}$$

Using the same approach as in Sec. II, the equations of motion for the laboratory experiment can be shown to have the form

$$\begin{aligned}&M_C\ddot\eta+\psi_B^T C^T\tilde S_B\dot\omega+\psi_B^T C^T\tilde\omega^T\tilde S_B\omega+\psi_B^T C^T\bar\Phi\ddot q+2\psi_B^T C^T\tilde\omega^T\bar\Phi\dot q\\&+\psi_B^T C^T(\tilde\omega^2+\dot{\tilde\omega}^T)\bar\Phi q+(m\psi_B^T+\bar\psi^T)g+K_C\eta=\psi_B^T C^T F\end{aligned} \tag{32a}$$

$$\begin{aligned}&I_B\dot\omega+\tilde\omega^T I_B\omega+\tilde S_B^T C\psi_B\ddot\eta+\bar\Phi\ddot q+[J(\dot\omega)+\tilde\omega^T J(\omega)\\&+[\widetilde{Cg}]\bar\Phi]q+[\tilde\omega^T\bar\Phi+J(\omega)]\dot q+\widetilde{Cg}]S_B=M\end{aligned} \tag{32b}$$

$$\begin{aligned}&M_A\ddot q+\bar\Phi^T C\psi_B\ddot\eta+\bar\Phi^T\dot\omega+\int_{m_A}\Phi^T\tilde\omega^T\tilde b\omega\,\mathrm{d}m_A+\bar\Phi^T Cg\\&+\tilde L_A(\omega)\dot q+[\tilde L_A(\omega)+\tilde L_A(\dot\omega)+K_A]q=Q\end{aligned} \tag{32c}$$

where $J(\omega)$ is redefined by replacing a with b in Eq. (19c) and

$$I_B=I_0+m\tilde e^T\tilde e+\tilde e^T\tilde S_0+\tilde S_0^T\tilde e \tag{33}$$

is the mass moment of inertia of the spacecraft about point B. In this case, only the Euler angles α_1, α_2, α_3 are assumed to be of arbitrary magnitude, and they are the ones responsible for many nonlinear terms in Eqs. (32).

IV. Perturbation Equations

The nonlinear equations of motion for the orbiting spacecraft have the same basic form as for the laboratory experiment. Hence, the approach to the solution suggested here applies for both situations.

Consider a first-order perturbation on the quantities R and α

$$R=R_0+R_1 \tag{34a}$$

$$\alpha=\alpha_0+\alpha_1 \tag{34b}$$

where the first-order terms R_1 and α_1 are small compared to the zero-order terms R_0 and α_0. Introducing Eqs. (34) into the nonlinear equations of motion, Eqs. (18) or (32), and separating orders of magnitude, we obtain zero-order and first-order perturbation equations. The zero-order equations can be used for maneuvering the spacecraft, and the first-order equations for vibration suppression and rigid-body corrections. Before proceeding with this technique, we first develop some expressions relating the perturbation vector α_1 in the Euler angles with the small angular deflection vector β expressed in the body-fixed frame. This is done so that all the variables in the perturbation equations can be expressed in the body-fixed frame, the frame in which state measurements are taken and actuating forces are applied.

First, consider Eq. (16), which relates the velocity vector $\dot\alpha$ in terms of the Euler angles to the body-fixed angular velocity vector ω. Introducing Eq. (34b) into Eq. (16) and neglecting higher-order terms, we obtain the perturbed angular velocity vector

$$\omega\simeq\omega_0+\omega_1 \tag{35}$$

where

$$\omega_0=D(\alpha_0)\dot\alpha_0 \tag{36a}$$

$$\omega_1=D(\alpha_1)\dot\alpha_0+D(\alpha_0)\dot\alpha_1 \tag{36b}$$

Using similar considerations, it can be shown that the body-fixed perturbation angles can be related to the perturbed Euler angles by the expression

$$\beta=D(\alpha_0)\alpha_1 \tag{37}$$

Note that the vector $\boldsymbol{\beta}$ is a first-order perturbation of a set of quasi-coordinates.[2] Taking the time derivative of Eq. (37) and introducing the result into Eq. (36b), it can be shown, after much algebra, that the perturbed angular velocity vector $\boldsymbol{\omega}_1$ is related to the angles $\boldsymbol{\beta}$ by the expression

$$\boldsymbol{\omega}_1 = \tilde{\omega}_0^T \boldsymbol{\beta} + \dot{\boldsymbol{\beta}} \tag{38a}$$

This result can be obtained in a much more straightforward manner. Because $\boldsymbol{\beta}$ is the first-order perturbation of the body-fixed quasi-coordinates and $\boldsymbol{\omega}_1$ is the vector of associated angular velocities, $\boldsymbol{\omega}_1$ must be the total time derivative of $\boldsymbol{\beta}$, or

$$\boldsymbol{\omega}_1 = \frac{\mathrm{d}\boldsymbol{\beta}}{\mathrm{d}t} = \boldsymbol{\omega}_0 \times \boldsymbol{\beta} + \dot{\boldsymbol{\beta}} \tag{38b}$$

which is equivalent to Eq. (38a). Taking the time derivative of Eq. (38a), the perturbed angular acceleration becomes

$$\dot{\boldsymbol{\omega}}_1 = \dot{\tilde{\omega}}_0^T \boldsymbol{\beta} + \tilde{\omega}_0^T \dot{\boldsymbol{\beta}} + \ddot{\boldsymbol{\beta}} \tag{39}$$

Next, we recall that the elements of the transformation matrix C from the body-fixed frame to the inertial frame consist of functions of the Euler angles, so that a perturbation of this matrix also involves the angles $\beta_1, \beta_2, \beta_3$. This relation can be derived using Eq. (38a). Instead, we consider the frame $0'$, which differs from the 0 frame by the angles $\beta_1, \beta_2, \beta_3$. Then, recalling that β_1, β_2, and β_3 are small, the transformation from the $0'$ frame to the 0 frame is $[I+\tilde{\beta}]$, where I is the identity matrix. Letting C_0 be the transformation matrix from the 0 frame to the inertial frame, the total transformation matrix C from the $0'$ frame to the inertial frame can be expressed as

$$C \cong C_0 + C_1 \tag{40}$$

where

$$C_1 = \tilde{\beta} C_0 \tag{41}$$

In keeping with our objective of expressing the first-order perturbation equations in the body-fixed frame, Eq. (34a) is replaced by

$$\boldsymbol{R} = \boldsymbol{R}_0 + C_0^T \boldsymbol{R}_1 \tag{42}$$

where $\boldsymbol{R}_1$ is now a vector measured with respect to the 0 frame. The control forces and moments can also be expressed in first-order perturbed form as follows:

$$\boldsymbol{F} = \boldsymbol{F}_0 + \boldsymbol{F}_1 \tag{43a}$$

$$\boldsymbol{M} = \boldsymbol{M}_0 + \boldsymbol{M}_1 \tag{43b}$$

Space Experiment

Introducing Eqs. (34–43) into Eqs. (18) and neglecting higher-order terms, we obtain two sets of equations of motion for the spacecraft in orbit. The zero-order equations, which govern the motion of the structure as if it were rigid, are

$$m\ddot{\boldsymbol{R}}_0 + C_0^T \tilde{S}_0 \dot{\omega}_0 + C_0^T \tilde{\omega}_0^T \tilde{S}_0 \omega_0 + \frac{Gm_e}{|\boldsymbol{R}_0|^3}[m\boldsymbol{R}_0 + (I - 3\hat{\boldsymbol{R}}_0 \hat{\boldsymbol{R}}_0^T) C_0^T S_0] = C_0^T F_0 \tag{44a}$$

$$\tilde{S}_0^T C_0 \ddot{\boldsymbol{R}}_0 + \frac{Gm_e}{|\boldsymbol{R}_0|^3} \tilde{S}_0^T C_0 \boldsymbol{R}_0 + I_0 \dot{\omega}_0 + \tilde{\omega}_0^T I_0 \omega_0 = M_0 \tag{44b}$$

where $\hat{\boldsymbol{R}}_0$ is a unit vector in the direction of $\boldsymbol{R}_0$. The first-order equations, which govern the small scale motions of the structure, can be expressed as

$$m\ddot{\boldsymbol{R}}_1 + 2m\tilde{\omega}_0^T \dot{\boldsymbol{R}}_1 + [\dot{\tilde{\omega}}_0^T + \tilde{\omega}_0^2 + \tilde{H}]\boldsymbol{R}_1 + \tilde{S}_0 \ddot{\boldsymbol{\beta}} + 2\tilde{\omega}_0^T \tilde{S}_0 \dot{\boldsymbol{\beta}} + [\dot{\tilde{\omega}}_0^T + \tilde{\omega}_0^2 + \tilde{H}]\tilde{S}_0 \boldsymbol{\beta} + \tilde{F}_0^T \boldsymbol{\beta} + \tilde{\Phi}\ddot{\boldsymbol{q}} + 2\tilde{\omega}_0^T \tilde{\Phi}\dot{\boldsymbol{q}} + [\dot{\tilde{\omega}}_0^T + \tilde{\omega}_0^2 + \tilde{H}]\tilde{\Phi}\boldsymbol{q} = \boldsymbol{F}_1 \tag{45a}$$

$$\tilde{S}_0^T \ddot{\boldsymbol{R}}_1 + 2\tilde{S}_0^T \tilde{\omega}_0^T \dot{\boldsymbol{R}}_1 + \tilde{S}_0^T [\dot{\tilde{\omega}}_0^T + \tilde{\omega}_0^2 + \tilde{H}]\boldsymbol{R}_1 + \tilde{F}_0 \boldsymbol{R}_1 + I_0 \ddot{\boldsymbol{\beta}} + [I_0 \tilde{\omega}_0^T + \tilde{\omega}_0^T I_0 + [\widetilde{I_0 \omega_0}]]\dot{\boldsymbol{\beta}} + [I_0 \dot{\tilde{\omega}}_0^T + \tilde{\omega}_0^T I_0 \tilde{\omega}_0^T + [\widetilde{I_0 \omega_0}]\tilde{\omega}_0^T + \tilde{S}_0 \tilde{H}]\boldsymbol{\beta} + \tilde{\Phi}\ddot{\boldsymbol{q}} + [\tilde{\omega}_0^T \tilde{\Phi} + J_0]\dot{\boldsymbol{q}} + [\dot{J}_0 + \tilde{\omega}_0^T J_0 + \tilde{H}\tilde{\Phi}]\boldsymbol{q} = M_1 \tag{45b}$$

$$\tilde{\Phi}^T \ddot{\boldsymbol{R}}_1 + 2\tilde{\Phi}^T \tilde{\omega}_0^T \dot{\boldsymbol{R}}_1 + \tilde{\Phi}^T [\dot{\tilde{\omega}}_0^T + \tilde{\omega}_0^2 + \tilde{H}]\boldsymbol{R}_1 + \tilde{\Phi}^T \ddot{\boldsymbol{\beta}} + [\tilde{\Phi}^T \tilde{\omega}_0^T - J_0^T]\dot{\boldsymbol{\beta}} + [\tilde{\Phi}^T \dot{\tilde{\omega}}_0^T - J_0^T \tilde{\omega}_0^T + \tilde{\Phi}^T \tilde{H}]\boldsymbol{\beta} + M_A \ddot{\boldsymbol{q}} + \tilde{L}_A \dot{\boldsymbol{q}} + [\tilde{L}_A + \dot{\tilde{L}}_A + K_A]\boldsymbol{q} = \boldsymbol{Q}_0 + \boldsymbol{Q}_1 \tag{45c}$$

where

$$\tilde{H} = \frac{Gm_e}{|\boldsymbol{R}_0|^3}[I - 3C_0 \hat{\boldsymbol{R}}_0 \hat{\boldsymbol{R}}_0^T C_0^T] \tag{46a}$$

$$\tilde{H} = \left[[\widetilde{C_0 \ddot{\boldsymbol{R}}_0}] + \frac{Gm_e}{|\boldsymbol{R}_0|^3}[\widetilde{C_0 \boldsymbol{R}_0}]\right] \tag{46b}$$

$$\boldsymbol{Q}_0 = -\left[\tilde{\Phi}^T C_0 \ddot{\boldsymbol{R}}_0 + \frac{Gm_e}{|\boldsymbol{R}_0|^3}\left(\tilde{\Phi}^T C_0 \boldsymbol{R}_0 + 3\widetilde{C_0 \boldsymbol{R}_0}\right] \bar{J} C_0 \frac{\hat{\boldsymbol{R}}_0}{|\boldsymbol{R}_0|}\right) + \tilde{\Phi}^T \dot{\omega}_0 + \int_{m_A} \Phi^T \tilde{\omega}_0^T \tilde{a} \omega_0 \mathrm{d}m_A\Big] \tag{46c}$$

Laboratory Experiment

For the laboratory experiment, the deflections of the cable (translation of the spacecraft) are assumed to be small. From purely rigid-body considerations, the point B (universal joint) must be close to the center of mass in the plane normal to the axis of rotation during a maneuver. Hence, the vector $\boldsymbol{S}_B$ can be considered to be small in the following analysis. Because the motion of the cable has been assumed to be small, introducing Eq. (36) into Eq. (32b), the zero-order equations for the laboratory experiment are simply

$$I_B \dot{\omega}_0 + \tilde{\omega}_0^T I_B \omega_0 = \boldsymbol{M}_0 \tag{47}$$

The motion of the cable, $\boldsymbol{w} = \psi\eta$, can be expressed with respect to the body-fixed frame, as in the case of the vector $\boldsymbol{R}_1$ for the orbiting spacecraft. Introducing Eqs. (36), (39–41), and (43) into Eqs. (32) and neglecting higher-order terms, the first-order equations of motion for the laboratory experiment can be expressed as follows:

$$M_C \ddot{\eta} + 2\tilde{L}_C \dot{\eta} + [\dot{\tilde{L}}_C + \tilde{L}_C + K_C]\eta + \psi_B^T \tilde{S}_B \ddot{\boldsymbol{\beta}} + 2\psi_B^T \tilde{\omega}_0^T \tilde{S}_B \dot{\boldsymbol{\beta}} + \psi_B^T [\dot{\tilde{\omega}}_0^T + \tilde{\omega}_0^2]\tilde{S}_B \boldsymbol{\beta} + \psi_B^T \tilde{\Phi}\ddot{\boldsymbol{q}} + 2\psi_B^T \tilde{\omega}_0^T \tilde{\Phi}\dot{\boldsymbol{q}} + \psi_B^T [\dot{\tilde{\omega}}_0^T + \tilde{\omega}_0^2]\tilde{\Phi}\boldsymbol{q} = \boldsymbol{F}_0 + \psi_B^T \boldsymbol{F} \tag{48a}$$

$$\tilde{S}_B^T \psi_B \ddot{\eta} + 2\tilde{S}_B^T \tilde{\omega}_0^T \psi_B \dot{\eta} + \tilde{S}_B^T [\dot{\tilde{\omega}}_0^T + \tilde{\omega}_0^2]\psi_B \eta + I_B \ddot{\boldsymbol{\beta}} + [I_B \tilde{\omega}_0^T + \tilde{\omega}_0^T I_B + (\widetilde{I_B \omega_0})]\dot{\boldsymbol{\beta}} + [I_B \dot{\tilde{\omega}}_0^T + \tilde{\omega}_0 I_B \tilde{\omega}_0 + (\widetilde{I_B \omega_0})\tilde{\omega}_0^T + \tilde{S}_B (\widetilde{C_0 g})]\boldsymbol{\beta} + \tilde{\Phi}\ddot{\boldsymbol{q}} + [\tilde{\omega}_0^T \tilde{\Phi} + J_0]\dot{\boldsymbol{q}} + [\dot{J}_0 + \tilde{\omega}_0^T J_0 + (\widetilde{C_0 g})\tilde{\Phi}]\boldsymbol{q} = M_0' + M_1 \tag{48b}$$

$$\tilde{\Phi}^T\psi_B\ddot{\eta}+2\tilde{\Phi}^T\tilde{\omega}_0^T\psi_B\dot{\eta}+\tilde{\Phi}^T(\dot{\tilde{\omega}}_0^T+\tilde{\omega}_0^2)\psi_B\eta$$
$$+\tilde{\Phi}^T\ddot{\beta}+[\tilde{\phi}^T\tilde{\omega}_0^T-J_0^T]\dot{\beta}+[\tilde{\Phi}^T\dot{\tilde{\omega}}_0^T-J_0^T\tilde{\omega}_0^T+\tilde{\Phi}^T(\widetilde{C_0g})^T]\beta$$
$$+M_A\ddot{q}+\tilde{L}_A\dot{q}+[\dot{\tilde{L}}_A+\dot{\tilde{L}}_A+K_A]q=Q_0+Q_1 \tag{48c}$$

where

$$F_0=-\psi_B^T(\tilde{\omega}_0^T\tilde{S}_B\omega_0+\tilde{S}_B\dot{\omega}_0)-[m\psi_B^T+\tilde{\psi}^T]C_0g \tag{49a}$$

$$M_0'=\tilde{S}_BC_0g \tag{49b}$$

$$Q_0=-\left(\tilde{\Phi}^T\dot{\omega}_0+\int_{m_A}\Phi^T\tilde{\omega}_0^T\tilde{b}\omega_0\mathrm{d}m_A+\tilde{\Phi}^TC_0g\right) \tag{49c}$$

V. First-Order Equations in Matrix Form

For the orbiting spacecraft, Eqs. (44) can be solved for $F_0(t)$ and $M_0(t)$ for any desired maneuver strategy $R_0(t)$ and $\omega_0(t)$. For the laboratory experiment, Eqs. (47) can be solved for $M_0(t)$ for any desired $\omega_0(t)$. In either case, these quantities can then be substituted into the first-order equations (45) or (48) to produce a set of linear equations with known time-varying coefficients governing the small deviations from the rigid-body maneuver and elastic motions of the structure. These linear equations can be expressed in the matrix form

$$M\ddot{x}+G\dot{x}+(K_S+K_{NS})x=F^* \tag{50}$$

where, for the orbiting case,

$$x^T=[R_1^T|\beta^T|q^T] \tag{51a}$$

$$F^{*T}=[F_1^T|M_1^T|Q_0^T+Q_1^T] \tag{51b}$$

$$M=\begin{bmatrix} M_0 & \tilde{S}_0 & \tilde{\Phi} \\ \tilde{S}_0^T & I_0 & \tilde{\Phi} \\ \tilde{\Phi}^T & \tilde{\Phi}^T & M_A \end{bmatrix} \tag{51c}$$

$$M_0=\begin{bmatrix} m & 0 & 0 \\ 0 & m & 0 \\ 0 & 0 & m \end{bmatrix} \tag{51d}$$

$$G=\begin{bmatrix} 2M_0\tilde{\omega}_0^T & 2\tilde{\omega}_0^T\tilde{S}_0 & 2\tilde{\omega}_0^T\tilde{\Phi} \\ -2(\tilde{\omega}_0^T\tilde{S}_0)^T & I_0\tilde{\omega}_0^T+\tilde{\omega}_0^TI_0+[\widetilde{I_0\omega_0}] & \tilde{\omega}_0^T\tilde{\Phi}+J_0 \\ -2(\tilde{\omega}_0^T\tilde{\Phi})^T & -[\tilde{\omega}_0^T\tilde{\Phi}+J_0]^T & 2\tilde{L}_A \end{bmatrix} \tag{51e}$$

$$K_S=\begin{bmatrix} M_0[\tilde{\omega}_0^2+\tilde{H}] & \tilde{F}_0^T+[\tilde{\omega}_0^2+\tilde{H}]\tilde{S}_0 & [\tilde{\omega}_0^2+\tilde{H}]\tilde{\Phi} \\ \tilde{F}_0+\tilde{S}_0^T[\tilde{\omega}_0^2+\tilde{H}] & \tilde{\omega}_0I_0\tilde{\omega}_0 & \tilde{\omega}_0^TJ_0+\tilde{H}\tilde{\Phi} \\ \tilde{\Phi}^T[\tilde{\omega}_0^2+\tilde{H}] & J_0^T\tilde{\omega}_0+\tilde{\Phi}^T\tilde{H}^T & \tilde{L}_A+K_A \end{bmatrix} \tag{51f}$$

$$K_{NS}=\begin{bmatrix} M_0\dot{\tilde{\omega}}_0^T & \dot{\tilde{\omega}}_0^T\tilde{S}_0 & \dot{\tilde{\omega}}_0^T\tilde{\Phi} \\ -(\dot{\tilde{\omega}}_0^T\ \tilde{S}_0)^T & I_0\dot{\tilde{\omega}}_0^T+[\widetilde{I_0\omega_0}]\tilde{\omega}_0^T+\tilde{S}_0\tilde{H} & \dot{J}_0 \\ -(\dot{\tilde{\omega}}_0^T\tilde{\Phi})^T & \tilde{\Phi}^T\dot{\tilde{\omega}}_0^T & \dot{\tilde{L}}_A \end{bmatrix} \tag{51g}$$

and, for the laboratory experiment,

$$x^T=[\eta^T|\beta^T|q^T] \tag{52a}$$

$$F^{*T}=[F_0^T+\psi_BF_1^T|M'^T_0+M_1^T|Q_0^T+Q_1^T] \tag{52b}$$

$$M=\begin{bmatrix} M_C & \psi_B^T\tilde{S}_B & \psi_B^T\tilde{\Phi} \\ \tilde{S}_B^T\psi_B & I_B & \tilde{\Phi} \\ \tilde{\Phi}^T\psi_B & \tilde{\Phi}^T & M_A \end{bmatrix} \tag{52c}$$

$$G=\begin{bmatrix} 2\tilde{L}_C & 2\psi_B^T\tilde{\omega}_0^T\tilde{S}_B & 2\psi_B^T\tilde{\omega}_0^T\tilde{\Phi} \\ -2(\psi_B^T\tilde{\omega}_0^T\tilde{S}_B)^T & I_B\tilde{\omega}_0^T+\tilde{\omega}_0^TI_B+[\widetilde{I_0\omega_0}] & \tilde{\omega}_0^T\tilde{\Phi}+J_0 \\ -2(\psi_B^T\tilde{\omega}_0^T\tilde{\Phi})^T & -[\tilde{\omega}_0^T\tilde{\Phi}+J_0]^T & 2\tilde{L}_A \end{bmatrix} \tag{52d}$$

$$K_S=\begin{bmatrix} \tilde{L}_C+K_C & \psi_B^T\tilde{\omega}_0^2\tilde{S}_B & \psi_B^T\tilde{\omega}_0^2\tilde{\Phi} \\ \tilde{S}_B^T\tilde{\omega}_0^2\psi_B & \tilde{\omega}_0I_B\tilde{\omega}_0 & \tilde{\omega}_0^TJ_0+[\widetilde{C_0g}]\tilde{\Phi} \\ \tilde{\Phi}^T\tilde{\omega}_0^2\psi_B & J_0^T\tilde{\omega}_0+\tilde{\Phi}^T[\widetilde{C_0g}]^T & \tilde{L}_A+K_A \end{bmatrix} \tag{52e}$$

$$K_{NS}=\begin{bmatrix} \dot{\tilde{L}}_C & \psi_B^T\dot{\tilde{\omega}}_0^T\tilde{S}_B & \psi_B^T\dot{\tilde{\omega}}_0^T\tilde{\Phi} \\ -(\psi_B^T\dot{\tilde{\omega}}_0^T\tilde{S}_B)^T & I_B\dot{\tilde{\omega}}_0^T+[\widetilde{I_B\omega_0}]\tilde{\omega}_0^T+\tilde{S}_B[\widetilde{C_0g}] & \dot{J}_0 \\ -(\psi_B^T\dot{\tilde{\omega}}_0^T\tilde{\Phi})^T & \tilde{\Phi}^T\dot{\tilde{\omega}}_0^T & \dot{\tilde{L}}_A \end{bmatrix} \tag{52f}$$

In both cases, the mass matrix is symmetric. For the orbiting structure, the mass matrix is time-invariant, whereas for the laboratory configuration it depends on time. This is the case because the mass matrix M_C of the cable is calculated with respect to the body-fixed frame and, hence, it is a function of the transformation matrix $C_0(t)$. Because the mass of the cable is much smaller than the mass of the spacecraft ($<0.8\%$), it can be regarded as negligible for certain purposes. Under these circumstances, M becomes time-invariant, as in the case of the orbiting spacecraft.

In both cases, the time-varying matrix G, multiplying the velocity vector, is skew-symmetric. This matrix contains the Coriolis (gyroscopic) terms.

The stiffness matrix has been split into two parts, one part K_S with purely symmetric terms, the other K_{NS} with the terms that lead to nonsymmetries. If desired, of course, K_{NS} can be separated into symmetric and skew-symmetric matrices. As can be seen in Eqs. (51g) and (52f), the terms containing the angular acceleration $\dot{\omega}_0$ of the body-fixed frame lead to nonsymmetric terms in the stiffness matrix. In fact, many of these terms are skew-symmetric, and hence circulatory. Note that the perturbation of the Euler equations resulted in some nonsymmetric terms containing only the angular velocity vector ω_0. This is not surprising because it is well known that a steady-state rigid-body rotation about the axis of intermediate moment of inertia is unstable.[27] Owing to the nonsymmetry of the stiffness matrices, the vibration problem is non-self-adjoint in both cases.

Because structural damping was ignored, the matrix G is due entirely to gyroscopic effects, and hence conservative in nature.[26] On the other hand, the stiffness matrix contains circulatory, nonconservative terms. During the maneuver, the centrifugal, tangential, and gravitational forces cause a change in the initial elastic deflection of the structure which, in

turn, affects the spacecraft's orientation. Therefore, the first-order vibration problem appears to be "self-excited" or, in a mathematical sense, non-self-adjoint. Active control is necessary to stabilize the zero-order maneuver, as well as to suppress the first-order vibrations.

According to Eqs. (47f) and (49f), the acceleration and velocity of the 0 frame during the maneuver produce tangential and centrifugal disturbance forces, which cause elastic motion. Of course, the elastic and rigid-body motions are coupled in the first-order equations, so that elastic deformations cause rigid-body deviations from the desired maneuver position. The control force vector $\boldsymbol{Q}_1$, which affects the elastic motion, contains contributions from the maneuver and vibration control. Hence, the optimal force distribution producing the desired maneuver should oppose the disturbance forces $\boldsymbol{Q}_0$ caused by the maneuver, minimizing the necessary vibration control effort.

VI. Maneuver Force Implementation for a Flexible Structure

The most desirable control technique designed to carry out a given maneuver is one that produces the desired rigid-body motion without exciting the elastic modes. The obvious approach is to apply a distributed force proportional to the rigid-body mode associated with the desired moment and weighted by the mass density. Because the modes are orthogonal with respect to the mass distribution, the other modes are not excited by this force. Of course, a distributed force can only be implemented approximately with discrete actuators, which tends to excite the other modes somewhat.

For simplicity, consider a rotation $\theta(t)$ about a principal axis. The governing equation for such a maneuver can be expressed as

$$M_0(t) = I_0 \ddot{\theta}(t) \tag{53}$$

where $\ddot{\theta}(t)$ is the desired angular acceleration, $M_0(t)$ the moment required to achieve the desired performance, and I_0 the mass moment of inertia about the rotational axis. For reasons mentioned above, we wish to apply the moment by means of distributed actuators, so that $M_0(t)$ is the resultant moment produced by forces $F(p,t)$ distributed throughout the structure or

$$M_0(t) = \int_D r(p) F(p,t) \mathrm{d}D \tag{54}$$

where $r(p)$ is the distance from the axis of rotation to a typical point p. Letting

$$I_0 = \int_D m(p) r^2(p) \mathrm{d}D$$

and introducing Eq. (54) into Eq. (53), the equation governing the maneuver can be expressed as

$$\int_D r(p) F(p,t) \mathrm{d}D = \int_D \ddot{\theta}(t) m(p) r^2(p) \mathrm{d}D \tag{55}$$

where $m(p)$ is the mass density of the structure at point p. In view of Eq. (55), the force density can be expressed as

$$F(p,t) = \ddot{\theta}(t) m(p) r(p) \tag{56}$$

Because it is proportional to the rotational mode weighted by the mass density, the force density represents a function orthogonal to all the other modes, so that it will excite only the desired rotational maneuver. Note that, because the force is also proportional to the mass, the mass acts as the control gain. This suggest that when this control force is implemented by means of discrete actuators, the actuators should be located at points of maximum mass for maximum efficiency in rigid-body control. Of course, analogously, torquers should be located at points characterized by maximum contribution to the mass moment of inertia.

When the rotational axis is not a principal axis, the required moments are given in Ref. 28 as

$$M_{01} = I_{11} \ddot{\theta} \tag{57a}$$

$$M_{02} = I_{21} \ddot{\theta} - I_{31} \dot{\theta}^2 \tag{57b}$$

$$M_{03} = I_{31} \ddot{\theta} + I_{21} \dot{\theta}^2 \tag{57c}$$

The moment vector can be expressed as

$$\boldsymbol{M}(t) = \int_D \boldsymbol{r}(p) \times \boldsymbol{F}(p,t) \mathrm{d}D \tag{58}$$

where

$$\boldsymbol{r}^T = [x \; y \; z] \tag{59a}$$

$$\boldsymbol{F}^T(p,t) = [F_1(p,t) \; F_2(p,t) \; F_3(p,t)] \tag{59b}$$

are the position vector and force vector, respectively, at a point on the body corresponding to mass density $m(p)$. Introducing the definition of the inertia matrix into Eqs. (57a–c) and comparing the resulting equations with Eq. (58), the distributed forces producing the desired moments can be expressed as

$$F_1(p,t) = x(p) m(p) \dot{\theta}^2(t) \tag{60a}$$

$$F_2(p,t) = -z(p) m(p) \ddot{\theta}(t) \tag{60b}$$

$$F_3(p,t) = y(p) m(p) \ddot{\theta}(t) \tag{60c}$$

As in the preceding analysis, the actuator forces are proportional to the rotational rigid-body modes and do not excite any other mode.

For a translational maneuver, the analysis is analogous to the one for rotational maneuvers. The force should be proportional to the corresponding translational mode so that the desired force can be expressed as

$$F(p,t) = a_0(t) m(p) \tag{61}$$

where $a_0(t)$ is the desired translational acceleration.

VII. Eigenvalue Problem: Reduction of Order

During the maneuver, the gyroscopic and stiffness matrices are functions of time. One could adopt an approach whereby the coefficient matrices are regarded as constant over small time steps and use the corresponding modal matrix to decouple the equations of motion. Solving the eigenvalue problem at each time step would be time-consuming. However, a truncated set of the premaneuver eigenvectors can be used as a set of admissible vectors to reduce further the number of equations of motion.

Equation (50) can be rewritten as

$$M\ddot{x}(t) + G(t)\dot{x}(t) + [K_0 + K_t(t)]x(t) = F^*(t) \tag{62}$$

where K_t consists of the time-varying and gravitational terms of the stiffness matrix and K_0 contains the remaining constant terms. The premaneuver equation of motion, neglecting gravity, can be expressed as

$$M\ddot{x}(t) + K_0 x(t) = F^*(t) \tag{63}$$

Table 1 Element material properties

	Stiffness			Inertia	
	Bending EI, lb-ft^2	Torsion GL, lb-ft^2	Axial EA, lb	Mass m/h, slugs/ft	Moment I_{xx}/m, ft^2
Cable	2.0	8.0	3.3120×10^{6}	0.01160	1.211×10^{-4}
Mast	1,648	1,263	3.9714×10^{6}	0.01391	8.302×10^{-4}
Antenna	557	411.65	1.3397×10^{6}	0.00475	8.327×10^{-4}

Table 2 Lumped masses attached to the shuttle

	Mass, slugs	Distance from point O		
		x, ft	y, ft	z, ft
Stack 1	4.3478	−0.8177	−1.5312	1.4895
Stack 2	4.3478	−0.8021	1.5625	1.4895
CMG	1.0640	3.0938	−0.0625	0.6615

Hence, the corresponding eigenvalue problem can be written in the form

$$K_0 x = \lambda M x \tag{64}$$

where $\lambda=\omega^2$ is an eigenvalue in which ω is a corresponding natural frequency and x is the associated eigenvector.

Owing to the nature of the discretization process, only the lower modes, say n modes, are accurate representations of the actual modes.[26] Of course, by increasing the number N of admissible functions in the original discretization process, we can increase the number n of accurate modes. The lower n modes can be arranged in the $N\times n$ matrix X of eigenvectors, which can be normalized so as to satisfy

$$X^T M X = I \tag{65a}$$

$$X^T K_0 X = \Lambda \tag{65b}$$

where I is the $n\times n$ identity matrix and Λ is the $n\times n$ diagonal matrix of eigenvalues. Using the expansion theorem,[26] the displacement vector for the premaneuver problem can be approximated by a linear combination of the lower n modes as follows:

$$x(t) = Xu(t) \tag{66}$$

where $u(t)$ is an n-vector of generalized coordinates. Inserting Eq. (66) into Eq. (62), premultiplying by X^T and considering Eqs. (65), we obtain

$$\ddot{u}(t) + \bar{G}(t)\dot{u}(t) + [\Lambda + \bar{K}(t)]u(t) = f(t) \tag{67}$$

where

$$\bar{G}(t) = X^T G(t) X, \tag{68a}$$

$$\bar{K}(t) = X^T K_t(t) X \tag{68b}$$

are the reduced-order gyroscopic and stiffness matrices and

$$f(t) = X^T F^*(t) \tag{69}$$

is a generalized force vector. The premaneuver eigenvectors have not decoupled the equations of motion. However, as the maneuver velocity decreases, the time-varying coefficients decrease in magnitude, and the equations approach their uncoupled form. Note that Eq. (67) is of order $2n<2N$, so that the equations of motion have been reduced in order. Also, the mass matrix has been reduced to the identity matrix, which is convenient for the next task of putting Eq. (67) in state space form. We refer to Eq. (67) as being in *quasi-modal form.*

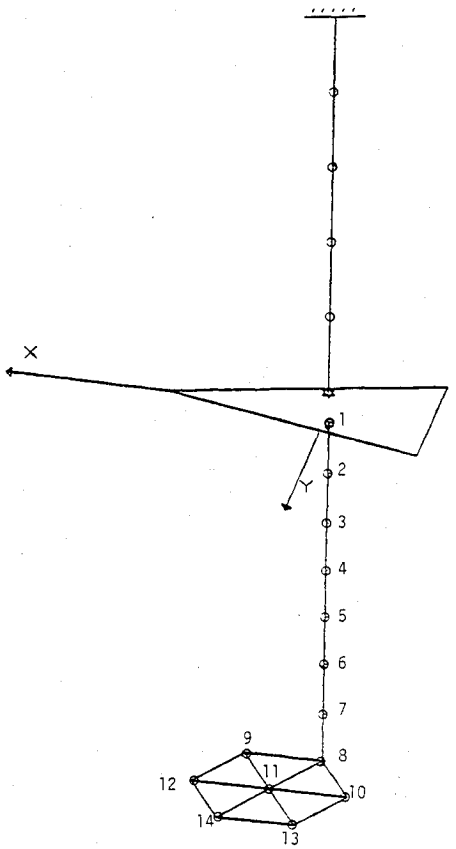

Fig. 3 Nodal locations for the SCOLE configuration.

VIII. Numerical Results

The SCOLE configuration of Fig. 2 is modeled by means of the finite-element method. The mast supporting the antenna is a steel tube 10 ft long. The antenna consists of 12 aluminum tubes, each 2 ft long, welded together to form a grid in a hexagonal shape. The tether is an 11-ft-long steel cable. The material properties can be found in Table 1. Figure 3 shows the nodal locations of the finite-element model. Hermite cubics were used as interpolation functions for bending and linear functions for axial and torsional deformations.

The "shuttle" is a steel plate of uniform thickness with a mass of 13.85 slugs. It is connected to the cable through a universal joint at point B. The $x_0y_0z_0$ frame is embedded in the shuttle, with the origin at its center of mass, as shown in Fig. 2. The center of mass is located 2.6708 ft from the rear of the shuttle in the x direction. Table 2 lists the values of the lumped masses attached to the plate and their respective locations. Table 3 identifies the location of the mast's attachment to the shuttle, as well as the universal joint's location, both with respect to the $x_0y_0z_0$ frame. Note that the mast is attached below the rigid-body center of mass and that the joint is located above the true center of mass. This joint location

provides a horizontal static equilibrium orientation for the shuttle that is the actual orientation for SCOLE. The total mass of the structure is 23.884 slugs, and the mass moment of inertia matrix about the universal joint is

$$I_B = \begin{bmatrix} 65.9409 & -0.006082 & 7.4305 \\ & 89.0227 & 2.1118 \\ \text{symm} & & 87.5150 \end{bmatrix} \text{slug-ft}^2$$

An eigensolution was obtained for the laboratory model of Fig. 2, with the structure in its static equilibrium state. The natural fequencies are listed in the first column of Table 4. Gravity forces have a great influence on the laboratory model. The natural frequencies of the spacecraft in a space environment, with no tether or gravitational effects, are listed in column 2 of Table 4. Note that there are now six zero frequencies corresponding to the rigid-body modes. All the frequencies are lower than the corresponding frequencies computed with the gravity effect included because gravity forces have a stiffening effect.

The maneuver strategy of Ref. 28 was applied to the rigid-body model of the spacecraft. The actuator response was assumed to be of first-order, with an exponential decay rate of 10.

The histories of two rotational maneuvers are presented. The discrete-time switching history of a 0-30-deg minimum-time rotation with $M_{\max} = 20$ lb-ft is illustrated in Fig. 4a. Note that the acceleration overshoots the target state because of the discrete-time switching. Figure 4b illustrates the continuous-time switching histories of 0-180-deg rotations with $M_{\max} = 60$ lb-ft, respectively. The effect of the actuator response is to smooth the curves at the switching states. If the actuator response is instantaneous, the acceleration is discontinuous.

Table 5 lists the eigenvalues of the spacecraft during the 180-deg maneuver. The vibration problem is non-self-adjoint during the maneuver, so that the real parts of the eigenvalues are nonzero during the rotation. Physically, this means that the initial configuration is not the equilibrium position during the rotation and, in fact, the equilibrium position is time-varying. Table 6 gives the natural frequencies.

Most of the nonsymmetric elements of the stiffness matrix, Eqs. (51g) and (52f), are functions of the angular acceleration. A positive real part of an eigenvalue corresponds to growth of that mode's participation in the vibration of the structure. Referring to Table 5, we observe that the participation of the flexible modes increases during the first half of the maneuver, when the angular acceleration is positive, and decreases during the second half. Note that the flexible modes most affected are the first two, modes 7 and 8.

The natural frequencies are also affected by the maneuvers. Most notably, the natural frequencies corresponding to four of the rigid-body modes are nonzero during the rotations. The natural frequencies of the flexible-body modes are also altered during the maneuver. Considering Eqs. (51f) and (52c), the stiffness matrix formed by terms involving only centrifugal accelerations and derived from the kinetic energy is negative semidefinite. On the other hand, the stiffness matrix of the appendage K_A includes centrifugal terms derived from the potential energy that are positive semidefinite.[26] Hence, the

Table 3 Mass and universal joint locations

	Distance from point O		
	x, ft	y, ft	z, ft
R.B. mass center	−0.1539	0.0116	0.4822
Mast attachment	−0.1539	0.0116	−0.3750
True mass center	−0.1546	0.0104	0.4817
Universal joint	−0.1546	0.0104	0.4937

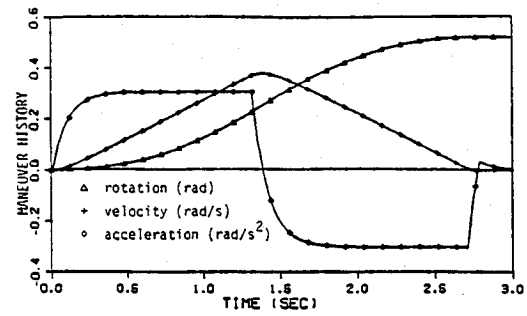

a) 30° roll, M_{max} = 20 ft-lb.

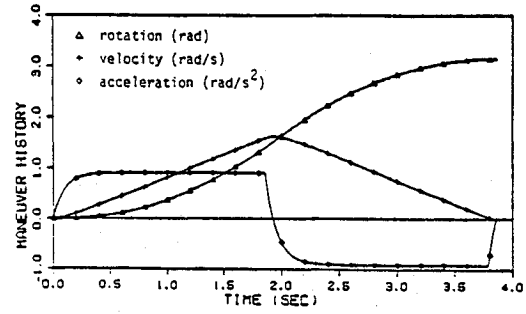

b) 180° roll, M_{max} = 60 ft-lb.

Fig. 4 Comparison of maneuver strategies.

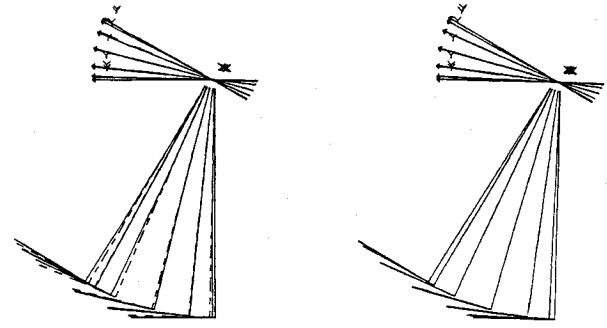

a) Actuators on shuttle b) Distributed actuators

Fig. 5 Time-lapse plots of 30-deg roll manevuer (FACT = 1.0).

Table 4 Natural frequencies, Hz

Mode	Equilibrium position	Zero gravity, space
1	0.0	0.0
2	0.0266	0.0
3	0.0334	0.0
4	0.2753	0.0
5	0.2753	0.0
6	1.0214	0.9563
7	1.0927	1.0221
8	2.8699	2.8580
9	4.1410	4.1224
10	7.2120	7.1357
11	11.8889	11.8067
12	11.9976	–
13	11.9980	–
14	14.5271	14.4703
15	17.8807	0.0
16	23.9952	–
17	23.9952	–
18	29.4619	29.3766
19	31.9790	31.8650
20	35.6083	35.5681

overall effect of the centrifugal terms on the natural frequencies is indefinite. The effects of the gyroscopic coefficients on the natural frequencies of an unsymmetric structure are also sign-indefinite. Of course, the fluctuations of the eigenvalues during the maneuver increase with the target angle and the acceleration rate.

Figure 5a is a time-lapse plot of the spacecraft during the 30-deg roll maneuver. The rotation is produced by actuators located on the shuttle, so that centrifugal and tangential forces cause structural vibration. The view is from directly behind the structure, showing the y_0z_0 plane with the x_0 axis directed into the paper. Two plots appear for each sampling time, one in dashed lines representing the structure as if it were rigid and the other representing the deformed structure. As the structure is accelerated, the appendage lags behind its desired position and then it bounces forward to precede the desired configuration during deceleration. When the maneuver ends, the appendage continues to vibrate about the desired target state. Note that the rigid-body error is small but discernible through the deflection of the y_0 axis. The quantity FACT given in the plots is the scale factor used to amplify the deformations for plotting purposes.

Figure 5b is also a time-lapse plot of the 30-deg roll. However, this time the maneuver was produced by actuators distributed throughout the structure. This form of actuation obviously causes a great deal less structural vibration. The distributed maneuver forces cancel the tangential disturbance forces, and only centrifugal forces remain to cause structural vibration. Hence, an increase in the number of actuators used to produce the rotational moments reduces the vibration caused by the maneuver. In fact, the use of just ten actuators, six on the shuttle and four thrusters, two located at the end of

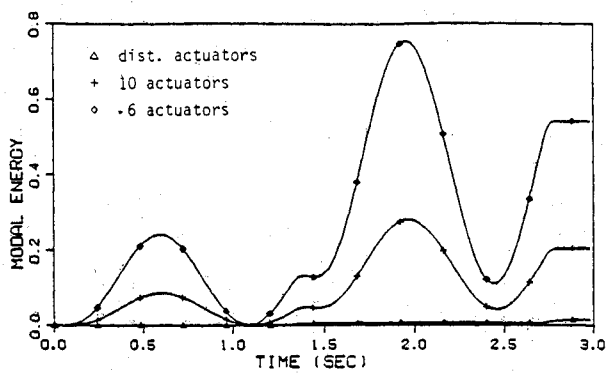

Fig. 6 Vibration energy during 30-deg maneuver with various numbers of actuators.

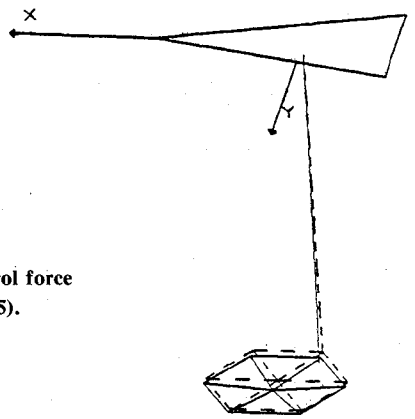

Fig. 7 Maneuver control force distribution (FACT = 7.5).

Table 5 Eigenvalues during 180-deg maneuver, $M_{max} = 60$ lb-ft

	Eigenvalues-real (rad/s)											
Time	Mode 1 $\times 10^3$	Mode 2 $\times 10^3$	Mode 3 $\times 10^3$	Mode 4 $\times 10^3$	Mode 5 $\times 10^3$	Mode 6 $\times 10^4$	Mode 7 $\times 10^4$	Mode 8 $\times 10^5$	Mode 9 $\times 10^5$	Mode 10 $\times 10^5$	Mode 11 $\times 10^5$	Mode 12 $\times 10^6$
0.00	0.00	0.00	0.00	0.00	0.00	0.00	0.00	0.00	0.00	0.00	0.00	0.00
0.35	0.85	2.03	−0.04	−0.04	0.85	0.24	0.24	1.07	1.07	0.51	0.51	1.08
0.70	2.08	4.68	−0.11	−0.11	2.08	0.59	0.59	2.62	2.62	1.24	1.24	2.63
1.05	3.28	6.84	−0.17	−0.17	3.28	0.93	0.93	4.15	4.15	1.96	1.96	4.17
1.40	4.46	−0.22	8.56	−0.22	4.46	1.28	1.28	5.68	5.68	269	2.69	5.71
1.75	−0.28	9.95	−0.28	5.62	5.62	1.62	1.62	7.21	7.21	3.41	3.41	7.25
2.10	0.24	−8.31	0.24	−4.75	−4.75	−1.36	−1.36	−6.10	−6.10	−2.88	−2.88	−6.13
2.45	0.24	−9.02	0.24	−4.67	−4.67	−1.33	−1.33	−5.95	−5.95	−2.81	−2.81	−5.98
2.80	0.18	−7.51	0.18	−3.52	−3.52	−1.00	−1.00	−4.45	−4.45	−2.11	−2.11	−4.48
3.15	2.32	−5.44	0.12	−0.12	−2.32	−0.66	−0.66	−2.93	−2.93	−1.38	−1.38	−2.99
3.50	0.06	−2.79	−1.11	0.06	−1.11	−0.31	−0.31	−1.39	−1.39	−0.66	−0.66	−1.40
3.85	0.00	0.00	0.00	0.00	0.00	0.00	0.00	0.00	0.00	0.00	0.00	0.00

Table 6 Natural frequencies (Hz)

	Eigenvalues-real (rad/s)											
Time	Mode 1	Mode 2	Mode 3 $\times 10^2$	Mode 4 $\times 10$	Mode 5 $\times 10$	Mode 6 $\times 10$	Mode 7 $\times 10$	Mode 8	Mode 9	Mode 10	Mode 11	Mode 12 $\times 10^{-1}$
0.00	0.00	0.00	0.00	0.00	0.00	0.00	9.56	1.02	2.86	4.12	7.14	1.18
0.35	0.00	0.00	6.91	0.83	1.29	1.42	9.56	1.02	2.86	4.12	7.14	1.18
0.70	0.00	0.00	2.04	0.55	1.64	1.94	9.54	1.03	2.86	4.13	7.14	1.18
1.05	0.00	0.00	2.72	0.03	2.00	2.45	9.51	1.03	2.86	4.14	7.14	1.18
1.40	0.00	0.00	0.00	0.81	2.38	2.96	9.48	1.04	2.86	4.15	7.14	1.18
1.75	0.00	0.00	2.39	1.32	2.78	0.35	9.45	1.05	2.86	4.17	7.15	1.18
2.10	0.00	0.00	3.79	1.49	2.76	3.44	9.44	1.05	2.86	4.17	7.15	1.18
2.45	0.00	0.00	0.48	0.91	2.45	3.05	9.47	1.04	2.86	4.15	7.14	1.18
2.80	0.00	0.00	2.20	0.40	2.07	2.55	9.51	1.03	2.86	4.14	7.14	1.18
3.15	0.00	0.00	1.05	0.50	1.71	2.04	9.54	1.03	2.86	4.13	7.14	1.18
3.50	0.00	0.00	6.12	0.79	1.37	1.54	9.56	1.02	2.86	4.12	7.14	1.18
3.85	0.00	0.00	2.97	0.30	0.30	0.30	9.56	1.02	2.86	4.12	7.14	1.18

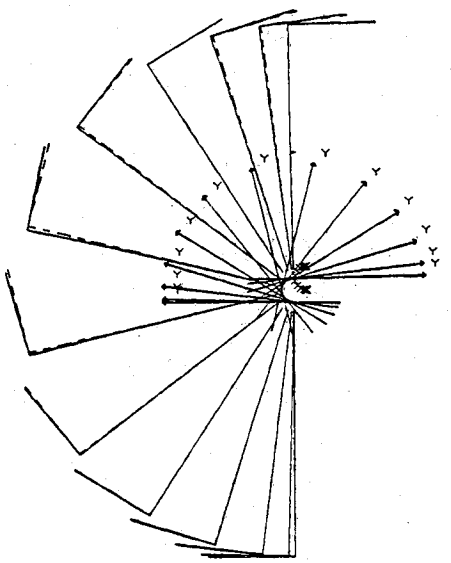

a) Time-lapse plot, FACT = 1.0

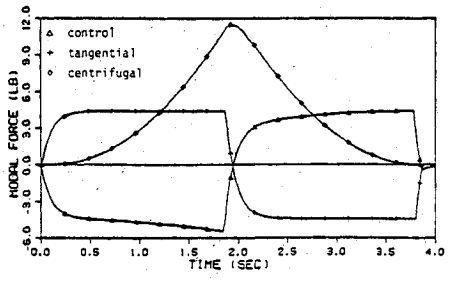

b) Modal disturbance and control forces

Fig. 8 Excitation of structures by centrifugal force during 180-deg roll.

the mast and two located at the hub of the antenna, decreases significantly the amount of energy imparted to the structure during the maneuver. Figure 6 shows a plot of the energy of the structure vs time for three cases, namely, distributed actuation, actuation approximating the distributed one with the above ten actuators, and six actuators located on the shuttle. Note that both the steady-state energy level and the instantaneous energy are decreased by the addition of actuators.

The location of the four thrusters used in the approximation to the distributed actuation discussed above were determined from a plot of the force distribution over the appendage for the case of distributed actuators. Figure 7 represents such a plot, where what appears to be the deformation of the appendage is actually the force distribution. The forces in the x_0 and y_0 directions at the hub of the antenna and the end of the mast contribute the most to the force distribution. Note that these locations have the highest mass concentration, which is no accident.

The maneuver and control techniques are now demonstrated for a more extreme situation, a 180-deg roll maneuver with $M_{max} = 60$ ft-lb. From Fig. 4b, we conclude that this is a relatively severe maneuver in that a 180-deg roll, starting and ending at rest, takes place in < 4 s. Also, the maximum angular velocity of the maneuver corresponds to 27% of the first flexible natural frequency. Moreoever, Table 5 shows that this maneuver alters the system eigenvalues significantly. Attempting this maneuver with actuators located only on the shuttle resulted in deformations of the appendage exceeding greatly the small elastic motions assumption. Figure 8a is a time-lapse plot of the structure during the maneuver in which the moments have been produced by distributed forces. The deformation is caused by the centrifugal disturbance force, which is much greater than for the 30-deg maneuver. The vibration problem during the maneuver is non-self-adjoint, and the eigensolution is time-varying.

The maneuver modal control forces, the tangential modal forces, and the centrifugal modal forces were each summed for all modes and plotted as functions of time in Fig. 8b. The control force cancels the tangential force, according to Eqs. (60b) and (60c), and opposes the rigid-body portion of the centrifugal forces, according to Eq. (60a). The remainder of the centrifugal force then excites vibration of the structure.

IX. Conclusions

The equations of motion for a maneuvering structure, both in orbit and in a laboratory environment, are nonlinear due to the large rigid-body motions. A perturbation method permits the development of a maneuver strategy independent of the vibration problem. The equations describing the vibration of the spacecraft during the maneuver are linear and non-self-adjoint with known time-dependent coefficients. Physically, this means that the equilibrium configuration does not correspond to the initial configuration during the maneuver and varies with time. Tangential and centrifugal disturbance forces cause vibration of the spacecraft during rotational maneuvers. A maneuver force distribution proportional to the rotational rigid-body mode minimizes the vibration caused by the maneuver by canceling the tangential disturbance forces. However, discrete actuation and centrifugal disturbance forces create a need for vibration control. The mass acts as the maneuver control force gain, so that discrete actuators should be placed at points of maximum mass for greatest efficiency. The vibration problem during the maneuver is non-self-adjoint, and the eigensolution is non-varying.

Acknowledgment

This research is supported by NASA Research Grant NAG-1-225 sponsored by the Spacecraft Control Branch, Langley Research Center. The grant is monitored by Mr. Jeffrey P. Williams.

References

[1]Meirovitch, L. and Nelson, H.D., "On the High-Spin Motion of a Satellite Containing Elastic Parts," *Journal of Spacecraft and Rockets,* Vol. 3, Nov. 1966, pp. 1597–1602.

[2]Hooker, W. and Margulies, G., "The Dynamical Attitude Equations for an n-Body Satellite," *Journal of Astronautical Sciences,* Vol. 12, 1965, pp. 123–128.

[3]Roberson, R.E. and Wittenburg, J., "A Dynamical Formalism for an Arbitrary Number of Interconnected Rigid Bodies with Reference to the Problem of Satellite Attitude Control," *Proceedings of the Third International Congress on Automatic Control,* Butterworth, London, England, 1967, pp. 45D.1–46D.8.

[4]Ho, J.Y.L. and Gluck, R., "Inductive Methods for Generating the Dynamic Equations of Motion for Multibodies Flexible Systems, Pt. 2, Perturbation Approach," *Synthesis of Vibrating System,* ASME, New York, 1971.

[5]Roberson, R.E., "A Form of the Translational Dynamical Equations for Relative Motion in Systems of Many Non-Rigid Bodies," *Acta Mechanica,* Vol. 14, 1972, pp. 297–308.

[6]Likins, P.W., "Dynamic Analysis of a System of Hinge-Connected Rigid Bodies With Non-Rigid Appendages," Jet Propulsion Laboratory, Pasadena, CA, Tech. Rept. 32-1576, 1974.

[7]Ho, J.Y.L., "Direct Path Method for Flexible Multibody Spacecraft Dynamics," *Journal of Spacecraft and Rockets,* Vol. 14, March–April 1977, pp. 102–110.

[8]Margulies, G., Auburn, J.N., Bushnell, D., and Ho, J.Y.L., "Multibody Flexible Spacecraft Integrated Analysis: Structures, Dynamics, and Control," *Proceeding of the First VPI&SU/AIAA Symposium on Dynamics and Control of Large Flexible Spacecraft,* edited by L. Meirovitch, Blacksburg, VA, 1977, pp. 437–456.

[9]Bodley, C.A., Devers, A., Park, A., and Frisch, H., "A Digital Computer Program for Dynamic Interaction Simulation of Controls and Structures (DISCOS)," *NASA Technical Paper 1219,* May 1978.

[10]Hurty, W.C., "Vibrations of Structural Systems by Component-Mode Synthesis," *Journal of Engineering Mechanics Division,* ASCE, Vol. 86, 1960, pp. 51–69.

[11]Hurty, W.C., "Dynamic Analysis of Structural Systems Using Component Modes," *AIAA Journal,* Vol. 3, April 1965, pp. 678–685.

[12]Craig, R.R. and Bampton, M.C.C., "Coupling of Substructures for Dynamic Analysis," *AIAA Journal,* Vol. 6, July 1968, pp. 1313-1319.

[13]Dowell, E.H., "Free Vibration of an Arbitrary Structure in Terms of Component Modes," *Journal of Applied Mechanics,* Vol. 39, No. 3, 1972, pp. 727-732.

[14]Meirovitch, L. and Hale, A.L., "Synthesis and Dynamic Characteristics of Large Structures with Rotating Substructures," *Proceedings of the IUTAM Symposium on the Dynamics of Multibody Systems,* edited by K. Magnus, Springer-Verlag, Berlin, FRG, 1978, pp. 231-244.

[15]Meirovitch, L. and Hale, A.L., "On the Substructure Synthesis Method," *AIAA Journal,* Vol. 19, July 1981, pp. 940-947.

[16]Meirovitch, L. ed., *Proceedings of the First VPI&SU/AIAA Symposium on Dynamics and Control of Large Flexible Spacecraft,* Blacksburg, VA, June 1977.

[17]Meirovitch, L. (ed), *Proceedings of the Second VPI&SU/AIAA Symposium on Dynamics and Control of Large Flexible Spacecraft,* Blacksburg, VA, June 1979.

[18]Meirovitch, L (ed.), *Proceedings of the Third VPI&SU/AIAA Symposium on Dynamics and Control of Large Flexible Spacecraft,* Blacksburg, VA, June 1981.

[19]Meirovitch, L. (ed), *Proceedings of the Fourth VPI&SU/AIAA Symposium on Dynamics and Control of Large Structures,* Blacksburg, VA, June 1983.

[20]Meirovitch, L. (ed), *Proceedings of the Fifth VPI&SU/AIAA Symposium on Dynamics and Control of Large Structures,* Blacksburg, VA, June 1985.

[21]Junkins, J.L. and Turner, J.D., "Optimal Continuous Torque Attitude Maneuvers," *Journal of Guidance and Control,* Vol. 3, May-June 1980, pp. 210-217.

[22]Turner, J.D. and Junkins, J.L., "Optimal Large-Angle Single-Axis Rotational Maneuvers of Flexible Spacecraft," *Journal of Guidance and Control,* Vol. 3, Nov.-Dec. 1980, pp. 578-585.

[23]Breakwell, J.A., "Optimal Feedback Slewing of Flexible Spacecraft," *Journal of Guidance and Control,* Vol. 4, Sept.-Oct. 1981, pp. 472-479.

[24]Turner, J.D. and Chun, H.M., "Optimal Distributed Control of a Flexible Spacecraft During a Large-Angle Maneuver," *Journal of Guidance, Control, and Dynamics,* Vol. 7, May-June 1984, pp. 257-264.

[25]Quinn, R.D., "Maneuver and Control of Flexible Spacecraft," Ph.D. Dissertation, Virginia Polytechnic Institute and State University, Blacksburg, VA, 1985.

[26]Meirovitch, L., *Computational Methods in Structural Dynamics,* Sijthoff & Noordhoff Co., The Netherlands, 1980.

[27]Meirovitch, L., *Methods of Analytical Dynamics,* McGraw-Hill, New York, 1970.

[28]Quinn, R.D. and Meirovitch, L., "Equations for the Vibration of a Slewing Flexible Spacecraft," *Proceedings of the AIAA/ASME/ASCE/AHS 27th Structures, Structural Dynamics and Materials Conference,* Pt. 2, AIAA, New York, 1986, pp. 342-354.